Global Nitrogen and Sulfur Deposition Mapping Using a Measurement-Model Fusion Approach

Hannah J. Rubin[1], Joshua S. Fu[1,2], Frank Dentener[3], Rui Li[4], Kan Huang[5], Hongbo Fu[5]

[1]Department of Civil and Environmental Engineering, University of Tennessee, Knoxville, TN, 37996, USA

[2]Computational Earth Science Group, Oak Ridge National Laboratory, Oak Ridge, TN 37831, USA

[3]European Commission, Joint Research Centre, Sipra, Italy

[4]Ministry of Education Key Laboratory for Earth System Modeling, Department of Earth System Science, Tsinghua University, Beijing, 100084, China

[5]Shanghai Key Laboratory of Atmospheric Particle Pollution and Prevention (LAP3), Department of Environmental Science and Engineering, Fudan University, Shanghai, 200433, China

E-mail: jsfu@utk.edu

Keywords: Measurement-model fusion, nitrogen deposition, sulphur deposition, HTAP II, ammonia, multiple-model mean

17 **Abstract**

18 Global reactive nitrogen (N) deposition has more than tripled since 1860 and is expected to

19 remain high due to food production and fossil fuel consumption. Global sulfur emissions have

20 been decreasing worldwide over the last 30 years, but many regions are still experiencing

21 unhealthily high levels of deposition. We update the 2010 global deposition budget for reactive

22 nitrogen and sulfur components with new regional wet deposition measurements from Asia,

23 improving the ensemble results of eleven global chemistry transport models from the second

24 phase of the United Nation's Task Force on Hemispheric Transport of Air Pollution (HTAP-II).

25 The observationally adjusted global N deposition budget is 114.5 Tg-N, representing a minor

26 increase of 1 % from the model-only derived values, and the adjusted global sulfur deposition

27 budget is 88.9 Tg-S, representing a 6.5% increase from the modelled values, using an

28 interpolation distance of 2.5 degrees. Regionally, deposition adjustments can be up to ~73% for

29 nitrogen, and 112% for sulfur. Our study demonstrates that a global measurement-model fusion

30 approach can improve N and S deposition model estimates at a regional scale, with sufficient

31 availability of observations, but in large parts of the world, alternative approaches need to be

32 explored. The analysis presented here represents a step forward toward the World

33 Meteorological Organization's goal of global fusion products for accurately mapping harmful air

34 pollution deposition.

35

36 **1. Introduction**

37 Atmospheric nitrogen and sulfur deposition from human activities related to the use of fossils

38 and land use have significant implications for ecosystem and human health. Elevated levels of

39 nitrogen and sulfur can lead to eutrophication (Anderson et al., 2008; Heisler et al., 2008),

40 changes in carbon sequestration (Kicklighter et al., 2019; de Vries et al., 2009; Zhu et al., 2020),

41 loss of biodiversity (Clark et al., 2013; Dise and Stevens, 2005), and acidification (Bowman et

42 al., 2008). While sulfur deposition is expected to decrease over the next 80 years (Lamarque et

43 al., 2013), it will remain a serious hazard in many emerging economies. For instance, sulfur

44 deposition in East Asia peaked in 2006 (Lu et al., 2010) but is still high enough to be concerning,

45 especially in natural and semi-natural regions (Doney et al., 2007; Luo et al., 2014).

46   Oxidized nitrogen (NO_y) and reduced nitrogen (NH_x), together called reactive nitrogen (Nr), and

47   oxidized sulfur (SO_x) deposition occur as wet and dry processes (Dentener et al., 2006). Wet

48   deposition is measured at hundreds of locations in Europe, North America, and Asia, but dry

49   deposition is harder to measure and is often instead derived from ambient concentrations and

50   modeled deposition velocities (Xu et al., 2015). For example, dry deposition is inferred from

51   continuous concentration measurements combined with modeled dry deposition velocities at a

52   few locations in North America (Clean Air Status and Trends Network (CASTNET), 2021) and

53   Asia (Acid Deposition Monitoring Network in East Asia (EANET), 2021).

54   The United Nations Economic Commission for Europe's Task Force on Hemispheric Transport

55   of Air Pollution (HTAP) is an international effort to improve the understanding of air pollution

56   transport science with emissions models. The second phase of HTAP was launched in 2012. Tan

57   et al. (2018) used the multi-model mean (MMM) of 11 HTAP II chemistry transport models to

58   estimate the sulfur and nitrogen deposition budgets for 2010. Significant uncertainty remained

59   due to a lack of station measurements, especially in East Asia, a large contributor to the overall

60   budget. Tan et al. (2018) compared Acid Deposition Monitoring Network in East Asia (EANET

61   (Acid Deposition Monitoring Network in East Asia, 2021)) measurements to the MMM output

62   but there were very few measurements in East Asia and all were located along the southeastern

63   coast. In contrast, the highest emissions and modeled deposition were inland and north, making it

64   challenging to evaluate model performance.

65   Combining measurements and model estimates in a "measurement-model fusion" (MMF)

66   approach has the advantage of retaining the broad spatial coverage of models while accurately

67   matching observations. Generally speaking, MMF takes model estimates of concentrations or

68   fluxes for a region and modifies them based on in-situ point measurements to force the model

69   towards the observed values (Labrador et al., 2020). One global MMF approach for wet

70   deposition combined measurements with HTAP I ensemble model values for 2000-2002 (Vet et

71   al., 2014) where model estimates filled empty grid cells lacking a 3-year observed mean.

72   Another MMF approach in North America (Atmospheric Deposition Analysis Generated from

73   optimal Interpolation from Observations, "ADAGIO") used observed concentrations to adjust

74   predicted concentrations from the Global Environmental Multiscale-Modelling Air Quality and

75   Chemistry (GEM-MACH) model (Schwede et al., 2019). Recent work in the US (Schwede and

76   Lear, 2014; Zhang et al., 2019) incorporates Community Multiscale Air Quality (CMAQ) model

77 output and precipitation data generated by the Parameter-elevation Regressions on Independent
78 Slopes Model (PRISM, https://prism.oregonstate.edu/, Accessed: 10/01/22), as well as
79 observations using inverse distance weighting to create total deposition ("TDep",
80 https://nadp.slh.wisc.edu/committees/tdep/#tdep-maps) maps that are publicly available.

81 More details of the MMF approach are described in Fu et al. (2022) as they lay out a roadmap
82 for future work, following the World Meteorological Organization's Global Atmosphere Watch
83 Program (WMO GAW) and the intended role of the MMF Global Total Atmospheric Deposition
84 (MMF-GTAD) project. This study updates Tan et al.'s (2018) global S and N deposition
85 budgets using a variation of the TDep methodology (Schwede and Lear, 2014) to merge NH_x,
86 NO_y, and SO_x modelled gridded deposition fluxes results with deposition fluxes derived from
87 observations of NO_3^-, NH_4^+, and SO_4^{2-} in precipitation and precipitation amounts The main
88 purpose of our study is to demonstrate the viability of a straightforward but globally applicable
89 MMF approach, while remaining consistent with previous work that provided datasets for impact
90 assessments for various communities. This approach is an important intermediate step towards
91 the WMO's goal of reliable deposition products to aid decision-making. We update the 2010
92 deposition budgets using MMF to combine the broad spatial coverage of a model with accurate
93 in-situ measurements.

94 **2. Data Availability**

95 **Table 1:** Sources of deposition observations.

Name	Source	Number of Observation Sites	Region	Value
NTN, AIRMoN	NADP	247	USA	wet deposition
CASTNET	NADP	84	USA	dry deposition
CAPMoN	NAtChem	27	Canada	wet and dry deposition
EMEP	EMEP	86	Europe	wet deposition
China Scientific Study	Li et al. 2019	407	China	wet deposition

EANET	EANET	47	East Asia	wet and dry deposition
IDAF	INDAAF	1	Niger	wet deposition

96

97 All data are from 2010, reported monthly with sources summarized in Table 1. Wet deposition

98 measurements (NO_3^-, NH_4^+, and SO_4^2) from the US's National Trends Network (NTN) and

99 Atmospheric Integrated Research Monitoring Network (AIRMoN) are available through the

100 National Atmospheric Deposition Program (NADP (National Atmospheric Deposition Program,

101 2021), http://nadp.slh.wisc.edu/NTN/). Measurements were filtered for completeness and quality,

102 following Schwede and Lear (2014). Sites without a full year of measurements or with quality

103 tags indicating collection issues were not included, resulting in 247 observations in the US. Dry

104 deposition generated values are available from the Clean Air Status and Trends Network

105 (CASTNET, 2021) at 84 locations. CASTNET uses an inferential method to calculate dry

106 deposition fluxes as a product of surface concentration and modeled dry deposition velocity.

107 Nitrogen and sulfur wet deposition measurements and dry deposition estimates throughout

108 Canada are recorded by the Canadian Air and Precipitation Monitoring Network (CAPMoN

109 (2021) and are available through the National Atmospheric Chemistry (NAtChem) database

110 (https://donnees.ec.gc.ca/data/air/monitor/). Dry deposition estimates from CAPMoN are

111 calculated by multiplying atmospheric concentration and deposition velocity. There were 27 sites

112 with a full year of quality checked data for 2010.

113 The European Monitoring and Evaluation Programme (EMEP (European Monitoring and

114 Evaluation Prgrarmme (EMEP), 2021; Tørseth et al., 2012), http://ebas-data.nilu.no/) provides

115 records of precipitation chemistry (NO_3^-, NH_4^+, and SO_4^{2-}) and precipitation depths for Europe.

116 There were 86 sites with a full year of quality checked data in 2010.

117 In China, a multi-year nationwide field study, including some of these NNDMN data, was

118 compiled by Li et al. (2019). Daily NO_3^-, NH_4^+, and SO_4^{2-} site measurements (in mg/L) were

119 averaged for 2010 for each of the 407 site locations with complete records by multiplying the

120 concentration by the precipitation recorded at that same site (in mm) and then aggregating to

121 produce annual precipitation-weighted deposition (Sirois, 1990). For a wider Asian region,

122 EANET (Asia Center for Air Pollution Research, 2021, https://www.eanet.asia/) wet and dry

123 deposition and precipitation data are available at 47 sites.

124 The International Global Atmospheric Chemistry (IGAC) Deposition of Biogeochemically

125 Important Trace Species (DEBITS) Africa (IDAF) program (Adon et al., 2010; Galy-Lacaux et

126 al., 2014) has NH_4^+ and NO_3^- precipitation concentrations on the International Network to Study

127 Deposition and Atmospheric Chemistry in Africa (INDAAF (INDAAF – International Network

128 to study Deposition and Atmospheric chemistry in AFrica, 2021)) website (https://indaaf.obs-

129 mip.fr/) for one site in Niger. All measurements were converted to mg-N (or S) /m^2/yr.

130

131 **3. Measurement Model Fusion Procedure**

132 Global yearly wet and dry NO_3^-, NH_4^+, and SO_4^{2-} deposition observations (for wet deposition) or

133 estimates derived from near-surface concentrations and modelled deposition velocities for dry

134 deposition) were combined with the respective HTAP II model average grid cell estimates, using

135 model output interpolated to common 1 degree x 1 degree (1° x 1°) grid cells (Figure 1). For

136 example, wet NO_3^- deposition observations are combined with the wet NO_3^- modeled deposition

137 in the nearest HTAP II MMM grid cell to the observation, where observations exist. Dry

138 deposition values (NO_3^-, NH_4^+, and SO_4^{2-}) from CASTNET and an inverse-distance weighted 1°

139 x 1° gridded dataset was created based on the distance from each observation to the center of the

140 nearest HTAP II model grid cell. Inverse-distance weighting (IDW) was selected as the most

141 straight forward to implement method to introduce MMF on a global scale while remaining

142 consistent with previous work (Schwede and Lear, 2014).

143 The weighting function was calculated as

144 $$\left(1 - \frac{distance}{max\ distance}\right)^2 \tag{1}$$

145 following Schwede and Lear's (Schwede and Lear, 2014) approach for the TDep product, where

146 "distance" is the distance between the site location and the center of the HTAP II model grid cell

147 nearest to that sampling site location, within a maximum distance of 2.5^o (approximately 280 km

148 at middle latitudes). The choice of the maximum distance is a crucial parameter for the inverse

149 distance weighting method in MMF. Prior analysis (e.g. Tan et al. 2018b) has shown that

150 gaseous and particulate sulfur and nitrogen emissions can travel several hundreds of kilometers,

151   before being deposited, although there is likely to be a large variation of transport distances due

152   to regional differences in chemistry, meteorological conditions, transport patterns and removal

153   processes. These processes interact with spatially heterogeneous emissions. Since there will not

154   be a single distance that captures the heterogeneity of all processes at play, we present here a

155   base case using a 2.5° interpolation distance, and two sensitivity cases reducing the distance to 1°

156   and increasing it to 5°, respectively. The 5° distance can be seen as an upper limit for the distance

157   where deposition observations can constrain deposition. The output values of the weighting

158   function at each observation location are then multiplied by the observed deposition. For the

159   center of every HTAP II model grid cell near that site, the modeled deposition is multiplied by 1

160   minus the value of the weighting function. Consequently, if there are no observations near the

161   model grid cells, the cell value remains the same. The two grid values ([weighting function times

162   observed deposition] and [1-weighting function times modeled deposition]) are added together to

163   give the value of the MMF estimate. This has the effect of modifying the HTAP II grid values

164   only in locations where there are observations within the maximum interpolation distance.

165   The MMF gridded surfaces were then summed by species along with the remaining unchanged

166   HTAP II gridded surfaces that lacked in-situ measurements to create total N and S deposition

167   gridded surfaces (e.g., the MMF wet and dry SO_4^- gridded surfaces were added to the HTAP II

168   wet and dry SO_2 gridded surfaces to get total S deposition). The MMF wet deposition surfaces

169   include measurements from Europe, Asia, and North America, and the dry deposition MMF

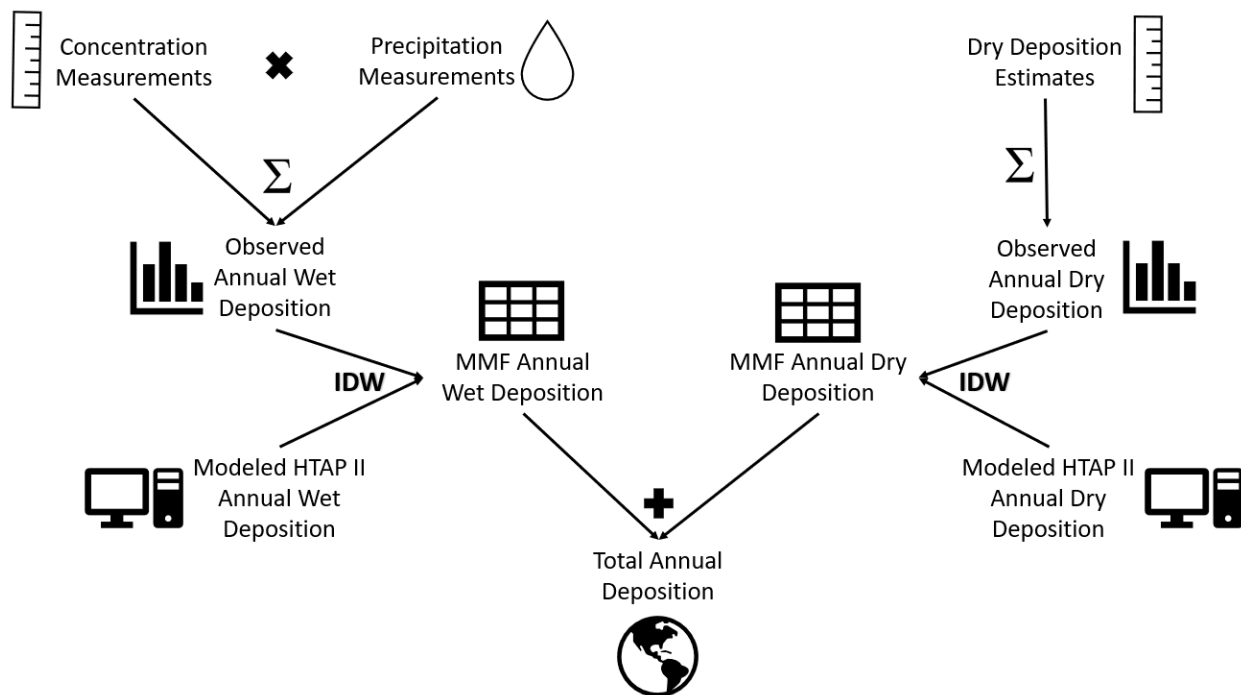170   surfaces include estimates from the USA and Asia (see section 2)

171

Concentration Measurements ✖ Precipitation Measurements

Σ

Observed Annual Wet Deposition

MMF Annual Wet Deposition

MMF Annual Dry Deposition

Dry Deposition Estimates

Σ

Observed Annual Dry Deposition

IDW

Modeled HTAP II Annual Wet Deposition

IDW

Modeled HTAP II Annual Dry Deposition

✚

Total Annual Deposition

172

173   **Figure 1. A flowchart describes the MMF methodology implemented in this paper.**

174

175   **4. Results**

176   The total global NH_x deposition in 2010 increased from 54.0 Tg-N (from HTAP II models) to

177   54.9 Tg-N (Table 2). Combined with a NO_y deposition of 59.6 Tg-N (from a modeled HTAP II

178   59.3 Tg-N), the total global deposition is adjusted to 114.5Tg-N (from 113 Tg-N), an increase by

179   1 %. While the IDW tends to decrease the depositions over the continents, an increase is

180   calculated over coastal regions and open oceans using the 2.5x2.5 maximum distance. Total S

181   deposition is adjusted to 88.91 Tg-S (Table 2), an increase by 6.5 % from the HTAP II model

182   prediction of 83.5 Tg-S (Figure 2B). Regional changes greater than or equal to 10% are bolded

183   and italicized.

184

185   **Table 2: 2010 adjusted global wet and dry deposition in Tg N or Tg S**, MMM indicates Tan et al.'s 2018 multi-

186   model mean and MMF is this measurement-model fusion work with a 2.5º interpolation distance. The 1º and 5º

187   interpolation distance results are shown in Tables S1 and S2. Coastal means deposition on sea within 1 degree of the

188   coastline. RBU is an abbreviation for Russia, Belarus, and Ukraine. Open ocean does not include near-land "coastal"

189   waters. The regions can be seen in the world map in Figure S1. Regional changes greater than or equal to 10% are

190   bolded and italicized.

| Region	Total NH$_x$				Total NO$_y$				Total SO$_x$			
	Non-Coastal		Coastal		Non-Coastal		Coastal		Non-Coastal		Coastal	
	MMM	MMF	MMM	MMF	MMM	MMF	MMM	MMF	MMM	MMF	MMM	MMF
North America	3.40	3.66	0.40	*0.31*	4.40	4.50	0.80	*0.94*	4.70	**5.67**	1.30	*1.69*
Europe	2.50	2.68	0.80	*1.14*	2.60	2.42	1.20	*1.75*	2.70	2.50	1.50	*3.18*
South Asia	8.60	8.60	1.00	1.00	3.60	3.60	0.70	0.70	3.70	3.70	1.00	1.00
East Asia	6.70	6.49	1.00	1.04	8.30	6.90	2.20	*2.45*	11.20	11.89	2.90	*4.10*
Southeast Asia	3.20	*2.22*	1.60	*2.12*	1.90	*1.60*	1.40	1.44	2.40	*0.81*	2.80	*0.56*
Australia	0.40	0.40	0.40	0.40	0.60	0.60	0.40	0.40	1.00	1.00	1.50	1.50
North Africa	0.70	0.70	0.20	0.20	1.40	1.40	0.40	0.40	1.00	1.00	0.50	0.50
Sub-Saharan Africa	3.40	3.40	0.40	0.40	4.70	4.70	0.60	0.60	2.70	2.70	0.70	0.70
Middle East	0.50	*0.38*	0.10	0.10	1.40	1.31	0.30	0.30	1.70	*3.18*	0.60	0.60
Central America	1.40	1.40	0.60	0.60	1.20	1.20	0.80	0.80	1.40	1.40	1.40	1.40
South America	3.80	3.80	0.30	0.30	3.40	3.40	0.30	0.30	2.40	2.40	0.60	0.60
RBU	1.80	*1.18*	0.30	*0.08*	2.40	*1.36*	0.50	0.47	3.60	**5.10**	0.90	*1.17*
Central Asia	0.50	*0.32*	0.00	0.00	0.60	0.55	0.00	0.00	1.20	*1.88*	0.10	0.10
Antarctica	0.10	0.10	0.00	0.00	0.10	0.10	0.00	0.00	1.40	1.40	0.00	0.00
Continental	37.00	35.33	7.10	7.69	36.70	33.64	9.70	10.55	41.00	44.63	15.60	*17.10*
Open Oceans	9.90	11.86			12.90	15.43			26.90	27.18		
Global	46.90	47.19	7.10	7.69	49.60	49.07	9.70	10.55	67.90	71.81	15.60	*17.10*

191
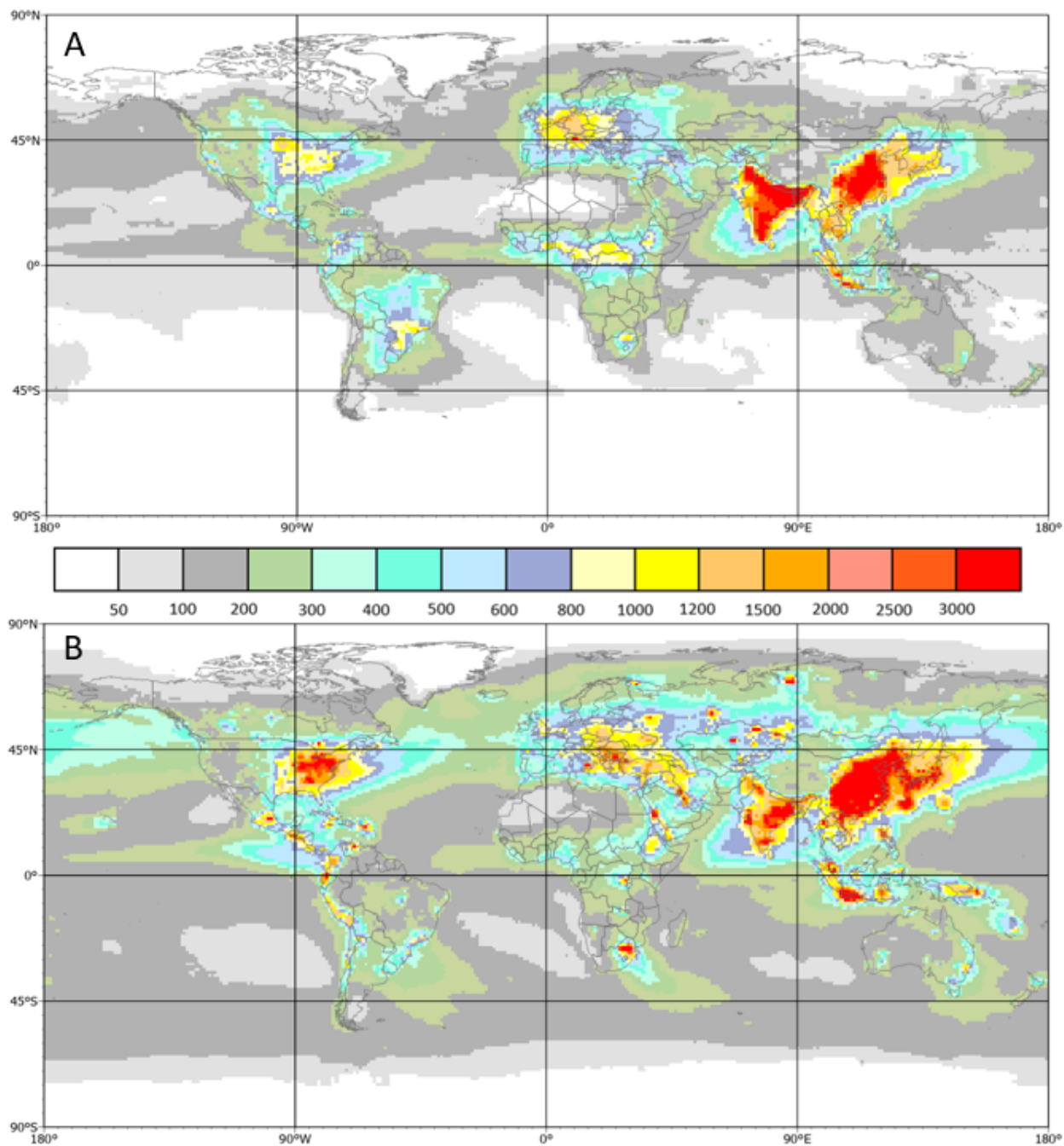
Figure 2: Total N and S deposition in 2010 using the MMF approach. A) Total annual N deposition (mg N/m^2), the sum of wet and dry NO$_3^-$ and NH$_4^+$ after applying the MMF approach, as well as HTAP II gridded surfaces of dry deposition of NH$_3$, HNO$_3$, and NO$_2$ with no MMF adjustment due to the lack of measurements. **B)** Total S deposition (mg S /m^2), the sum of wet and dry MMF SO$_4^{2-}$ and wet and dry HTAP II SO$_2$.

197
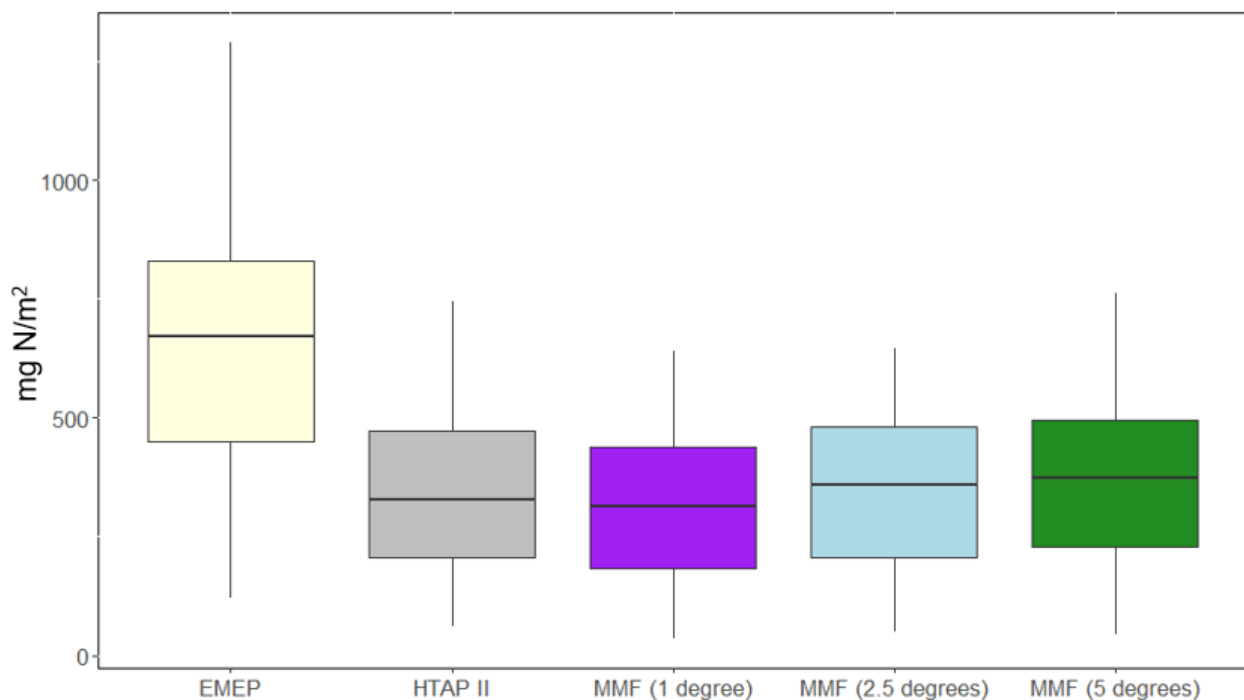
Figure 3: A comparison between HTAP II, MMF, and EMEP wet deposition fluxes in Europe results at

EMEP observation sites. A boxplot shows the distribution of EMEP, HTAP II, and MMF modeled wet reactive

nitrogen deposition (NH_x and NO_y) results at each EMEP observation location. Three different interpolation

distances are compared using MMF, 1 degree, 2.5 degrees, and 5 degrees.

Tan et al. (2018) report that their MMM underestimates the high observations of total N

deposition at some EMEP stations in Europe. We find that our 2.5º interpolation value for

European wet N deposition (8.0 Tg) is increased by 12.5% relative to the MMM surface (7.1

Tg), although the distance to the observations remains high (Figure 3). Figures 4, S4 and S5

show the difference between HTAP-II MMM and MMF nitrogen and sulfur deposition in North

America, Europe, and Asia in mg/m^2 with different interpolation distances. As the interpolation

distance increases, locations with a single measurement that is very different from the model will

influence the surrounding grid cells to be higher than the model. This effect is in particular

pronounced for sulfur deposition in Southeast Asia (Figure 4 B3) where the MMF procedure

increases deposition by up to 250 mg/m^2 relative to the MMM values.
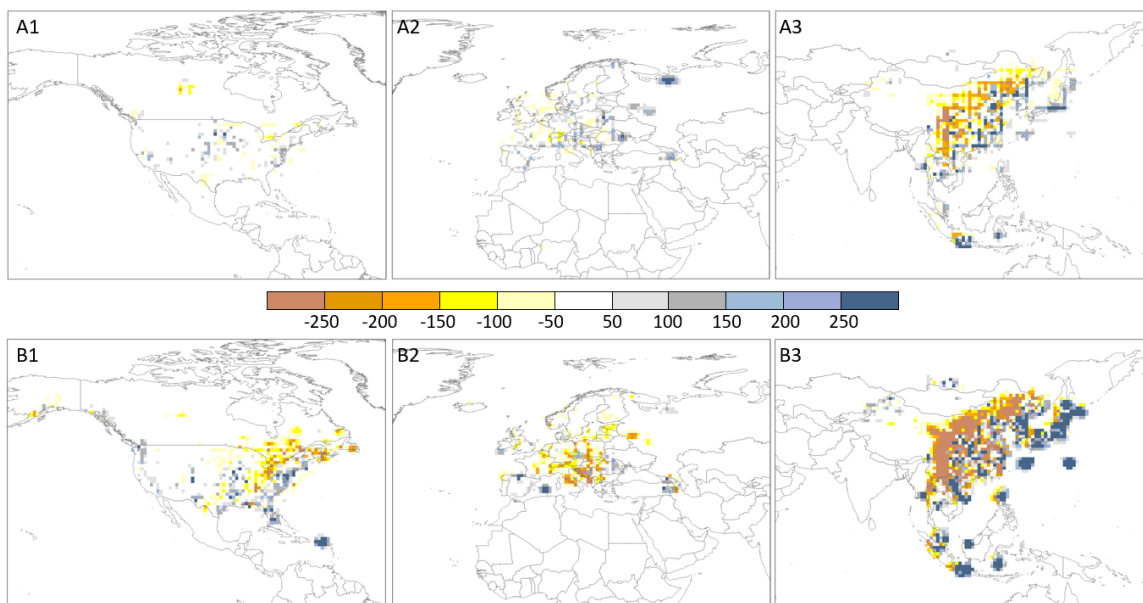
Figure 4. The difference between MMF and MMM deposition with a 2.5-degree interpolation distance. **A)** MMF minus MMM reactive nitrogen deposition in North America (**A1**) Europe (**A2**) and East Asia (**A3**) in mg N/m^2. **B**) MMF minus MMM sulfate deposition in North America (**B1**) Europe (**B2**) and East Asia (**B3**) in mg S/m^2. Results for other interpolation distances are shown in Figures S4 and S5, respectively.

The spatial distribution is slightly different, with more deposition in coastal areas in the MMF estimate (Table 2). Tan et al. (2018) report that the HTAP II MMM overestimates NO_3^- wet deposition in North America, but underestimates NH_4^+ deposition. We find that the MMF interpolated deposition slightly improves these estimates, although the spatial distribution is very similar with the MMM (Figures 2, 5). The largest change for S deposition (comparing MMM and MMF) is in grid cells classified as ocean because of an increase in East and Southeast Asia deposition which mostly occurs in areas classified as ocean due to the small island size relative to the coarse spatial resolution of the models. We note that, ocean cells were classified as such if they were located further than 1º from the mainland; therefore, any islands smaller than 1º were counted as the ocean.
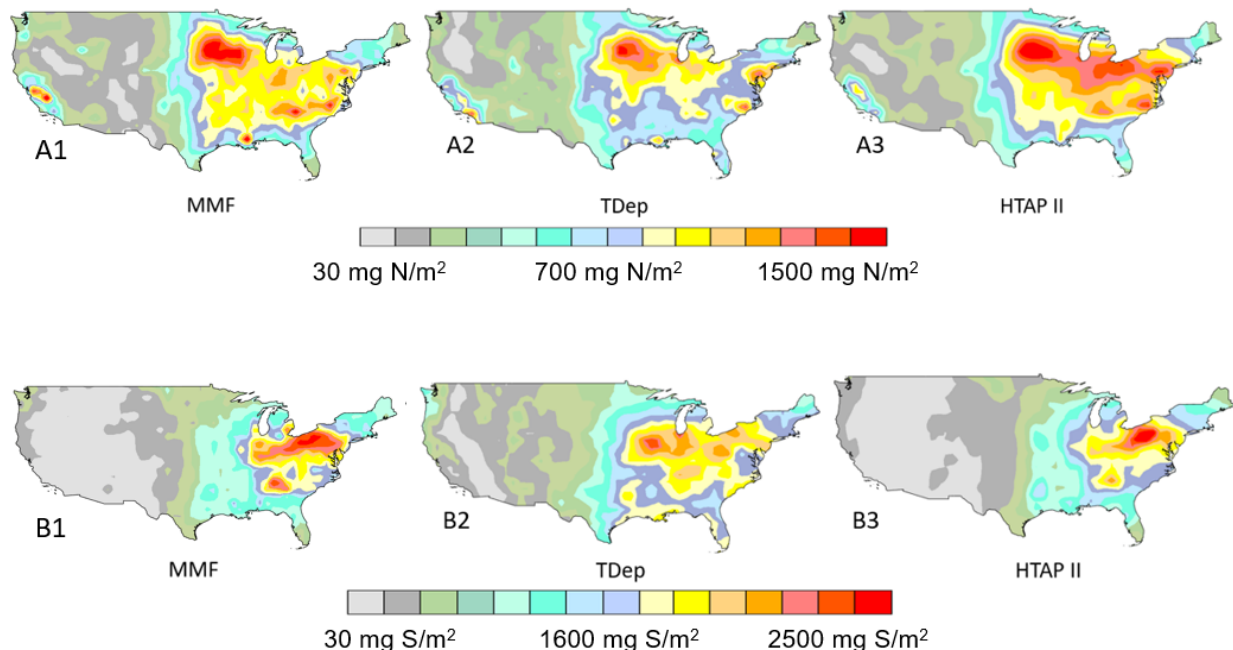
Figure 5: 2010 Total N deposition in the continental USA. **A**) Total N is modeled with 1) MMF (this work), 2) TDep annual map available from the NADP and 3) Tan et al.'s 2018 MMM. **B**) 2010 SO_x wet deposition in the US as modeled with 1) MMF (this work), 2) TDep annual map available from the NADP, and 3) Tan et al.'s 2018 multi-model mean HTAP II output.

There are spatial differences between an aggregated 1° x 1° version of the original TDep map of nitrogen deposition for the United States as available from the NADP (Figure 5A2), the HTAP II (Figure 5A3) deposition produced by Tan et al. (2018) corresponding to the same area, and the deposition map produced in this work (Figure 5A1). A similar pattern is seen in the map of SO_4^{2-} deposition (Figure 5B1; 5B3;5B3). While the TDep maps have been aggregated to the 1x1 degree resolution of the HTAP fields, there is still different regional variation in the deposition patterns in the TDep maps than the HTAP II maps. In particular, TDep is capturing higher west coast values that HTAP II does not while showing lower values in the Midwest/New York/Pennsylvania region.

The R^2 value for the linear regression between MMF wet SO_4^{2-} and observed wet SO_4^{2-} in the US is 0.64 (Figure 6). The R^2 value for the linear regression between the HTAP II wet SO_4^{2-} and observed SO_4^{2-} is 0.0.60, and 0.89 for the linear regression between the TDep wet SO_4^{2-} and observed SO_4^{2-} (Figure 6). This means that TDep is better reproducing the NADP/NTN

250　measurements and their spatial differences, whereas the MMF fields remain more similar to the

251　HTAP II ensemble model output. The higher TDep R^2 value likely occurs because of the finer

252　mesh (12 km) used in the TDep product, the closer proximity to individual stations as compared

253　to HTAP II used in the MMF approach, and the ability of the regional model to capture

254　gradients. In principle, emissions should be the same but in global models they are averaged over

255　larger areas. All three datasets produce similar values to the measured wet SO_x deposition at the

256　NADP/NTN sites (Figure 6). The NH_4 and NO_3 wet deposition values are shown in Figures S2

257　and S3, and have much lower correlations (for all three interpolation distances), with an R^2 of 0.1

258　for NO_3 and 0.53 for NH_4 at a 2.5º weighted distance

259
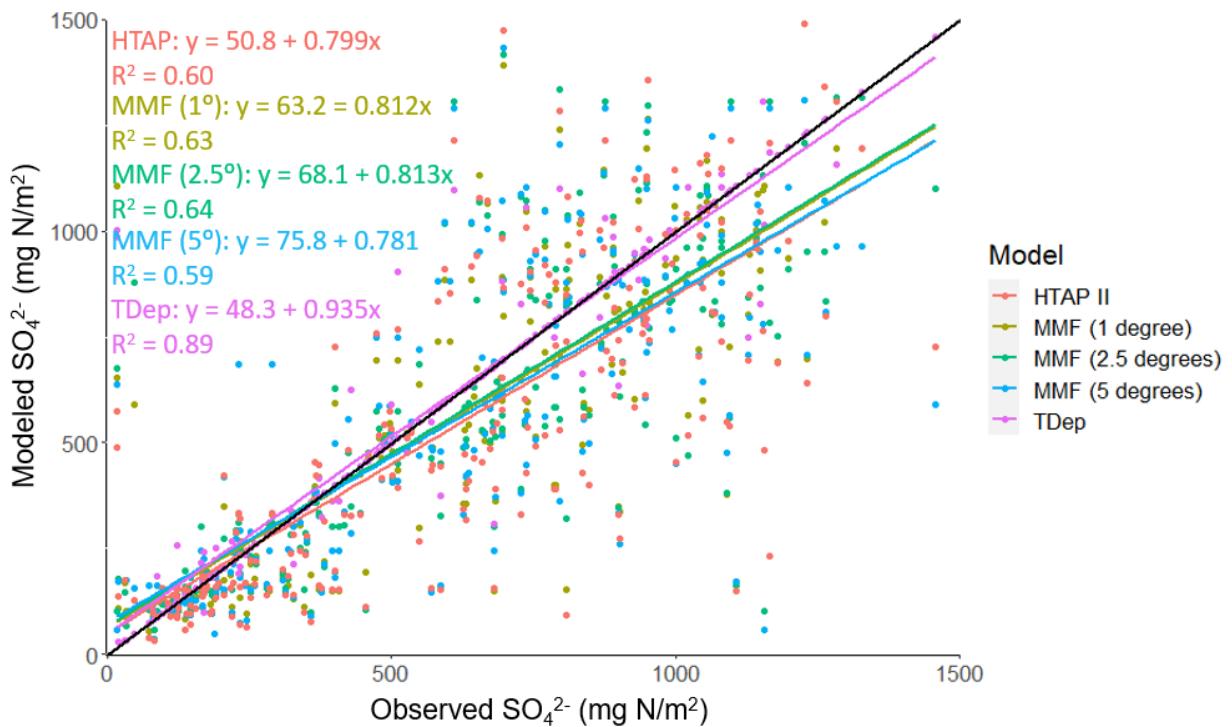
Figure 6: Observed and modeled wet SO_4^{2-} deposition in the US in 2010. Each NADP/NTN wet deposition measurement and the associated HTAP II, TDep, or MMF NH_x wet deposition modeled value, with all values shown together in A. The black line is the 1:1 line. Similar plots are shown in Figures S2 and S3 for wet NO_3 and wet NH_4.

5. Discussion

5.1 Consistency of MMF deposition with global emission estimates.

268   Geddes et al. (2017) used satellite observations to report global NO_y emissions of 57.5 Tg-N/yr

269   in 2010, similar to the 60.4 Tg-N emissions reported by HTAP II. This matches well with our

270   total global MMF-derived NO_y deposition (58.1 Tg-N). HTAP II ammonia emissions were 59.3

271   Tg-N, slightly lower than the MMF NH_3 and NH_4+ deposition of 62.3 Tg-N. The total MMM

272   sulfur emissions for 2010 were 90.7 Tg S, very similar to the MMF sulfur deposition of 88.9 Tg-

273   N.

274   *5.2 Deposition over China.*

275   A promising data set of wet deposition measurements (NO_3^-, NH_4^+, and SO_4^{2-}) in China is

276   available through the National Nitrogen Deposition Monitoring Network (NNDMN (Xu et al.,

277   2019)). It is comparable to other regional measurements (Wen et al., 2020). However, these data

278   only exist for a fraction of 2010 (from September onwards) for a few sites; rather than use partial

279   data to represent an entire year, these sites were not included in our study. Research in China

280   (Liu et al., 2020) analyzed the spatial pattern of N deposition by combining satellite observations

281   with NNDMN deposition measurements (Xu et al., 2019); they found a 2012 average of 18.21 kg

282   N ha^{-1} for China? Additional work combining the GEOS-Chem

283   (http://acmg.seas.harvard.edu/geos/) model with satellite observations and surface measurements

284   reports the average annual deposition from 2008-2012 as 16.4 Tg-N with 10.2 Tg-N from NH_x

285   and 6.2 Tg-N from NO_y (Zhao et al., 2017). The averages reported by these studies are consistent

286   with ours (16.9 kg ha^{-1} yr^{-1}) despite the difference in year and spatial resolution. The spatial

287   pattern of N deposition in 2010 (Figure 2A) also remains similar to that of previous decades (Jia

288   et al., 2014), with high deposition in eastern China and low deposition over the Tibetan Plateau.

289   This pattern is confirmed in 2006 and 2013 (Qu et al., 2017).

290   *5.3 Limitations of interpolation*

291   As seen in Table 2, the largest difference between MMM and MMF is found in coastal regions

292   and particularly the open ocean. While MMF does give improved deposition estimates by

293   incorporating in-situ measurements, it is worth considering the scale of the model. Observations

294   of deposition are probably not everywhere representative for a 1º or larger resolution and

295   observations of precipitation may also not be homogenous in all directions at that scale,

296   especially over heterogeneous terrain. So, for example, the coarse resolution of the model, even

297   with added measurements is likely not accurately capturing gradients between coastal and inland

298   deposition. While higher resolution precipitation values are available in some regions (e.g.,

299   PRISM in the US), there is still a dearth of both wet and dry deposition measurements. Even on

300   the North American continental scale, Schwede et al. (2011) showed that partially overlapping

301   dry deposition estimates from CASTNET (USA) and CAPMoN (Canada)can be very different,

302   despite using similar methodologies. This adds uncertainty to the dry deposition data (though

303   there are very few dry deposition estimates included in this study) and emphasizes the

304   importance of understanding deposition velocity model methodology.

305   The differences between the TDep, MMM, and MMF gridded deposition (Figure 5) are clearly

306   visible in the center of the US. While the general patterns of deposition are similar for the three

307   products, the magnitude of deposition in the aggregated TDep dataset (1° x 1°) is higher in the

308   eastern US and lower in the western US than either of the other two deposition fields. This

309   difference is likely due to the precipitation dataset used to calculate wet deposition. The MMF

310   deposition is based on the MMM dataset; therefore, both utilize the same precipitation dataset,

311   from a combination of 11 global models. However, TDep wet deposition is produced by

312   multiplying PRISM precipitation data and an interpolated gridded surface dataset of wet NH_4^+

313   concentrations. PRISM is a reanalysis product designed to interpolate precipitation in

314   particularly complex landscapes using weather radar and rainfall gauge observations, though it is

315   not identical to observations because it used long-term averages as predictor grids (Zhang et al.,

316   2018). It captures much more localized variation in precipitation due to geographical variations

317   which are not captured in the lower resolution global precipitation models used in the HTAP II

318   MMM (Tan et al., 2018a). To illustrate this, we compare PRISM to the available Community

319   Atmosphere Model with Chemistry (https://www2.acom.ucar.edu/gcm/cam-chem, "CAM-

320   Chem"), which was one of the models in the HTAP II ensemble. Subtracting the CAM-Chem

321   precipitation output over the US from aggregated PRISM precipitation shows that CAM-Chem

322   greatly underestimates precipitation volume in the US in 2010 (Figure S6). We note, however,

323   that this comparison does not take differences in precipitation frequency between the model and

324   observations into account. This matters because if the difference in precipitation volume comes

325   from a few large magnitude storms, it will not influence the overall wet deposition values much.

326   This is a good example of the differences that occur when comparing global and regional climate

327   models and serves to emphasize the importance of resolving spatial and temporal scales. The

328   total deposition within the US borders is similar for the MMF, HTAP II, and aggregated TDep

329   gridded surfaces; however, the spatial distribution is different.

330   MMF and MMM deposition distributions are similar because MMF is based on HTAP II.

331   Likewise, the MMF results are similar to the TDep values at observation locations because,

332   despite the difference in precipitation, both utilize the same NADP/NTN measurements to

333   constrain the models. The key difference between MMF, when compared to MMM, is that

334   measurement locations are not centered in each 1° x 1° grid cell; therefore, the center of each grid

335   cell (the value compared to the observation, by interpolation to the station location) will not

336   exactly equal the measured deposition but will instead be equal to the measurements weighted

337   proportionally to distance from the centroid. This means that the graphical comparison of Figure

338   6 is showing the actual measurement locations and 3 different model results with some

339   meaningful influence from measurements that are nonetheless unique values, except in the very

340   rare instance that the measurement corresponds exactly to the center of a grid cell. Figure 6

341   shows a stronger correlation for SO_4 than Figures S2 and S3 do for the nitrogen species. This

342   could be related to the relatively shorter timescales of NO_y and NH_x in the atmosphere. The

343   relatively coarse resolution of the global models cannot deal with these gradients, so the shorter

344   timescales are reflected in the observations which are therefore less representative for the larger

345   grid scales of the models.

346   TDep maps of North American nitrogen deposition created with Schwede and Lear's

347   methodology (2014), using IDW, are widely in use and freely available from the NADP. The

348   sensitivity analysis demonstrates that as the interpolation distance increases, the influence of the

349   observations on the HTAP II grid increases, smoothing some of the artifacts that can occur using

350   a small interpolation distance (Figures 6, S2, S3). In this respect it is worth mentioning that the

351   original TDep dataset for North America used a maximum distance of 30 km plus half the cell

352   size of PRISM (2.07 km). While it is not entirely clear how this distance was determined,

353   operational factors such as the station density and the grid size of the regional model are likely

354   important factors. In contrast, the maximum distances explored in this study are much larger (1°,

355   2.5^o, 5°) and are more adapted to the grid size of the current generation of global atmospheric

356   chemistry transport models, and considerations of transport distances of atmospheric

357   components. From our analysis there is no obvious better weighting distance that improves the

358   comparison with observations. An adaptive distance weighting that considers the expected

359 gradients between the observation point and the remote model grid could be explored as a way

360 forward.

361 However, there are strong limitations associated with using IDW (Sahu et al., 2010), and other

362 interpolation methods such as kriging or geographically weighted regression could provide

363 smoother surfaces with fewer artifacts. IDW is a fast and flexible interpolation method, but it

364 does not minimize error and can produce inaccurate results in regions with sparse measurements

365 and large sub-grid variability. This problem is relevant to much of the world. The lack of

366 measurement sites globally is a hindrance that can be alleviated by including information

367 obtained from satellite remote sensing (Walker et al., 2019). Future work should also investigate

368 methods such as machine learning techniques with spatial information to avoid these limitations.

369 These results from measurement-model fusion are important because previous methods on a

370 global scale have relied primarily on models (Vet et al., 2014; Tan et al., 2018a). They compare

371 their results with measurements, of course, in order to demonstrate the model capabilities but

372 they do not explicitly incorporate point measurements into the final product. Our results serve to

373 emphasize that global models are adequately simulating deposition (in terms of total deposition

374 budgets) but that the regional discrepancies between models and measurements can still be quite

375 large; and measurement-model fusion helps to ameliorate this without changing the fundamental

376 model parameters and processes that actually capture the overall deposition reasonably well.

377 **6. Conclusions**

378 Sulfur and nitrogen deposition remain a serious concern for human and ecosystem health. We

379 update the 2010 deposition budgets using measurement-model fusion to combine the broad

380 spatial coverage of a model with accurate in-situ measurements. The total nitrogen deposition

381 budget is recalculated to 114.50 Tg-N and the sulfur budget is recalculated to 88.91 Tg-N,

382 representing about a 1% and 6.5% increase, respectively, from the modelled values. This work

383 emphasizes the necessity of combining models with observations wherever possible, to better

384 capture regional patterns and to inform policy and decision-making. Future work to improve

385 measurement-model fusion should investigate more advanced MMF methods to avoid the

386 limitations associated with IDW such as surface artifacts and high error in regions with sparse

387 measurements. It could also incorporate satellite remote sensing derived concentrations to

388 improve model estimates where in-situ measurements are not available, but a careful error

389 analysis is needed to avoid spurious results.

390 **Author Contribution**

391 HR carried out the methods and analyzed the results. JSF and FD designed the project. HR

392 prepared the manuscript with contributions from JSF and FD. RL, KH, and HF provided data.

393 **Competing Interests**

394 The authors declare no competing interests.

395 **Code Availability**

396 Data analysis was done using ArcMap Desktop 10.8.1, ArcGIS Pro, and R (R Core Team, 2022).

397

398   **References**

399   Adon, M., Galy-Lacaux, C., Yoboué, V., Delon, C., Lacaux, J. P., Castera, P., Gardrat, E.,
400   Pienaar, J., Al Ourabi, H., Laouali, D., Diop, B., Sigha-Nkamdjou, L., Akpo, A., Tathy, J. P.,
401   Lavenu, F., and Mougin, E.: Long term measurements of sulfur dioxide, nitrogen dioxide,
402   ammonia, nitric acid and ozone in Africa using passive samplers, Atmos. Chem. Phys., 10,
403   7467–7487, https://doi.org/10.5194/acp-10-7467-2010, 2010.

404   Anderson, D. M., Burkholder, J. M., Cochlan, W. P., Glibert, P. M., Gobler, C. J., Heil, C. A.,
405   Kudela, R. M., Parsons, M. L., Rensel, J. E. J., Townsend, D. W., Trainer, V. L., and Vargo, G.
406   A.: Harmful algal blooms and eutrophication: Examining linkages from selected coastal regions
407   of the United States, Harmful Algae, 8, 39–53, https://doi.org/10.1016/j.hal.2008.08.017, 2008.

408   Acid Deposition Monitoring Network in East Asia (EANET): https://www.eanet.asia/, last
409   access: 18 November 2021.

410   Bobbink, R., Hicks, K., Galloway, J., Spranger, T., Alkemade, R., Ashmore, M., Bustamante,
411   M., Cinderby, S., Davidson, E., Dentener, F., Emmett, B., Erisman, J.-W., Fenn, M., Gilliam, F.,
412   Nordin, A., Pardo, L., and Vries, W. D.: Global assessment of nitrogen deposition effects on
413   terrestrial plant diversity: a synthesis, Ecological Applications, 20, 30–59,
414   https://doi.org/10.1890/08-1140.1, 2010.

415   Bowman, W. D., Cleveland, C. C., Halada, Ĺ., Hreško, J., and Baron, J. S.: Negative impact of
416   nitrogen deposition on soil buffering capacity, Nature Geoscience, 1, 767–770,
417   https://doi.org/10.1038/ngeo339, 2008.

418   Clark, C. M., Bai, Y., Bowman, W. D., Cowles, J. M., Fenn, M. E., Gilliam, F. S., Phoenix, G.
419   K., Siddique, I., Stevens, C. J., Sverdrup, H. U., and Throop, H. L.: Nitrogen Deposition and
420   Terrestrial Biodiversity, in: Encyclopedia of Biodiversity, Elsevier, 519–536,
421   https://doi.org/10.1016/B978-0-12-384719-5.00366-X, 2013.

422   Dentener, F., Drevet, J., Lamarque, J. F., Bey, I., Eickhout, B., Fiore, A. M., Hauglustaine, D.,
423   Horowitz, L. W., Krol, M., Kulshrestha, U. C., Lawrence, M., Galy-Lacaux, C., Rast, S.,
424   Shindell, D., Stevenson, D., Noije, T. V., Atherton, C., Bell, N., Bergman, D., Butler, T., Cofala,
425   J., Collins, B., Doherty, R., Ellingsen, K., Galloway, J., Gauss, M., Montanaro, V., Müller, J. F.,
426   Pitari, G., Rodriguez, J., Sanderson, M., Solmon, F., Strahan, S., Schultz, M., Sudo, K., Szopa,
427   S., and Wild, O.: Nitrogen and sulfur deposition on regional and global scales: A multimodel
428   evaluation, Global Biogeochemical Cycles, 20, https://doi.org/10.1029/2005GB002672, 2006.

429   Dise, N. B. and Stevens, J.: Nitrogen deposition and reduction of terrestrial biodiversity:
430   Evidence from temperate grasslands, Sci. China Ser. C.-Life Sci., 48, 720–728,
431   https://doi.org/10.1007/BF03187112, 2005.

432   Doney, S. C., Mahowald, N., Lima, I., Feely, R. A., Mackenzie, F. T., Lamarque, J.-F., and
433   Rasch, P. J.: Impact of anthropogenic atmospheric nitrogen and sulfur deposition on ocean
434   acidification and the inorganic carbon system, PNAS, 104, 14580–14585,
435   https://doi.org/10.1073/pnas.0702218104, 2007.

436 European Monitoring and Evaluation Prgrarmme (EMEP): https://www.emep.int/, last access: 18
437 November 2021.

438 Canadian Air and Precipitation Monitoring Network: https://www.canada.ca/en/environment-
439 climate-change/services/air-pollution/monitoring-networks-data/canadian-air-precipitation.html,
440 last access: 18 November 2021.

441 Fu, J. S., Carmichael, G. R., Dentener, F., Aas, W., Andersson, C., Barrie, L. A., Cole, A., Galy-
442 Lacaux, C., Geddes, J., Itahashi, S., Kanakidou, M., Labrador, L., Paulot, F., Schwede, D., Tan,
443 J., and Vet, R.: Improving Estimates of Sulfur, Nitrogen, and Ozone Total Deposition through
444 Multi-Model and Measurement-Model Fusion Approaches, Environ. Sci. Technol., 56, 2134–
445 2142, https://doi.org/10.1021/acs.est.1c05929, 2022.

446 Galy-Lacaux, C., Delon, C., Solmon, F., Adon, M., Yoboué, V., Mphepya, J., Pienaar, J. J.,
447 Diop, B., Sigha, L., Dungall, L., Akpo, A., Mougin, E., Gardrat, E., and Castera, P.: Dry and Wet
448 Atmospheric Nitrogen Deposition in West Central Africa, in: Nitrogen Deposition, Critical
449 Loads and Biodiversity, edited by: Sutton, M. A., Mason, K. E., Sheppard, L. J., Sverdrup, H.,
450 Haeuber, R., and Hicks, W. K., Springer Netherlands, Dordrecht, 83–91,
451 https://doi.org/10.1007/978-94-007-7939-6_10, 2014.

452 Geddes, J. A. and Martin, R. V.: Global deposition of total reactive nitrogen oxides from 1996 to
453 2014 constrained with satellite observations of NO_2 columns, Atmospheric Chemistry and
454 Physics, 17, 10071–10091, https://doi.org/10.5194/acp-17-10071-2017, 2017.

455 Heisler, J., Glibert, P. M., Burkholder, J. M., Anderson, D. M., Cochlan, W., Dennison, W. C.,
456 Dortch, Q., Gobler, C. J., Heil, C. A., Humphries, E., Lewitus, A., Magnien, R., Marshall, H. G.,
457 Sellner, K., Stockwell, D. A., Stoecker, D. K., and Suddleson, M.: Eutrophication and harmful
458 algal blooms: A scientific consensus, Harmful Algae, 8, 3–13,
459 https://doi.org/10.1016/j.hal.2008.08.006, 2008.

460 INDAAF – International Network to study Deposition and Atmospheric chemistry in AFrica:
461 https://indaaf.obs-mip.fr/, last access: 18 November 2021.

462 Jia, Y., Yu, G., He, N., Zhan, X., Fang, H., Sheng, W., Zuo, Y., Zhang, D., and Wang, Q.:
463 Spatial and decadal variations in inorganic nitrogen wet deposition in China induced by human
464 activity, Sci Rep, 4, 3763, https://doi.org/10.1038/srep03763, 2014.

465 Kicklighter, D. W., Melillo, J. M., Monier, E., Sokolov, A. P., and Zhuang, Q.: Future nitrogen
466 availability and its effect on carbon sequestration in Northern Eurasia, Nat Commun, 10, 3024,
467 https://doi.org/10.1038/s41467-019-10944-0, 2019.

468 Labrador, L., Volosciuk, C., and Cole, A.: Measurement-Model Fusion for Global Total
469 Atmospheric Deposition, a WMO initiative, World Meteorological Organization, 2020.

470 Lamarque, J.-F., Dentener, F., McConnell, J., Ro, C.-U., Shaw, M., Vet, R., Bergmann, D.,
471 Cameron-Smith, P., Dalsoren, S., Doherty, R., Faluvegi, G., Ghan, S. J., Josse, B., Lee, Y. H.,
472 MacKenzie, I. A., Plummer, D., Shindell, D. T., Skeie, R. B., Stevenson, D. S., Strode, S., Zeng,
473 G., Curran, M., Dahl-Jensen, D., Das, S., Fritzsche, D., and Nolan, M.: Multi-model mean

nitrogen and sulfur deposition from the Atmospheric Chemistry and Climate Model Intercomparison Project (ACCMIP): evaluation of historical and projected future changes, Atmos. Chem. Phys., 13, 7997–8018, https://doi.org/10.5194/acp-13-7997-2013, 2013.

Li, R., Cui, L., Zhao, Y., Zhang, Z., Sun, T., Li, J., Zhou, W., Meng, Y., Huang, K., and Fu, H.: Wet deposition of inorganic ions in 320 cities across China: spatio-temporal variation, source apportionment, and dominant factors, Atmospheric Chemistry and Physics, 19, 11043–11070, https://doi.org/10.5194/acp-19-11043-2019, 2019.

Liu, L., Zhang, X., Xu, W., Liu, X., Zhang, Y., Li, Y., Wei, J., Lu, X., Wang, S., Zhang, W., Zhao, L., Wang, Z., and Wu, X.: Fall of oxidized while rise of reduced reactive nitrogen deposition in China, Journal of Cleaner Production, 272, 122875, https://doi.org/10.1016/j.jclepro.2020.122875, 2020.

Lu, Z., Streets, D. G., Zhang, Q., Wang, S., Carmichael, G. R., Cheng, Y. F., Wei, C., Chin, M., Diehl, T., and Tan, Q.: Sulfur dioxide emissions in China and sulfur trends in East Asia since 2000, Atmos. Chem. Phys., 10, 6311–6331, https://doi.org/10.5194/acp-10-6311-2010, 2010.

Luo, X. S., Tang, A. H., Shi, K., Wu, L. H., Li, W. Q., Shi, W. Q., Shi, X. K., Erisman, J. W., Zhang, F. S., and Liu, X. J.: Chinese coastal seas are facing heavy atmospheric nitrogen deposition, Environ. Res. Lett., 9, 095007, https://doi.org/10.1088/1748-9326/9/9/095007, 2014.

National Atmospheric Deposition Program: https://nadp.slh.wisc.edu/, last access: 18 November 2021.

Qu, L., Xiao, H., Zheng, N., Zhang, Z., and Xu, Y.: Comparison of four methods for spatial interpolation of estimated atmospheric nitrogen deposition in South China, Environ Sci Pollut Res, 24, 2578–2588, https://doi.org/10.1007/s11356-016-7995-0, 2017.

R Core Team: R: A Language and Environment for Statistical Computing, 2022.

Sahu, S. K., Gelfand, A. E., and Holland, D. M.: Fusing point and areal level space–time data with application to wet deposition, Journal of the Royal Statistical Society: Series C (Applied Statistics), 59, 77–103, https://doi.org/10.1111/j.1467-9876.2009.00685.x, 2010.

Schwede, D., Zhang, L., Vet, R., and Lear, G.: An intercomparison of the deposition models used in the CASTNET and CAPMoN networks, Atmospheric Environment, 45, 1337–1346, https://doi.org/10.1016/j.atmosenv.2010.11.050, 2011.

Schwede, D., Cole, A., Vet, R., and Lear, G.: Ongoing U.S. - Canada Collaboration on Nitrogen and Sulfur Deposition, 5, 2019.

Schwede, D. B. and Lear, G. G.: A novel hybrid approach for estimating total deposition in the United States, Atmospheric Environment, 92, 207–220, https://doi.org/10.1016/j.atmosenv.2014.04.008, 2014.

508   Sirois, A.: The effects of missing data on the calculation of precipitation-weighted-mean
509   concentrations in wet deposition, Atmospheric Environment. Part A. General Topics, 24, 2277–
510   2288, https://doi.org/10.1016/0960-1686(90)90321-D, 1990.

511   Tan, J., Fu, J. S., Dentener, F., Sun, J., Emmons, L., Tilmes, S., Sudo, K., Flemming, J., Jonson,
512   J. E., Gravel, S., Bian, H., Davila, Y., Henze, D. K., Lund, M. T., Kucsera, T., Takemura, T., and
513   Keating, T.: Multi-model study of HTAP II on sulfur and nitrogen deposition, Atmospheric
514   Chemistry and Physics, 18, 6847–6866, https://doi.org/10.5194/acp-18-6847-2018, 2018a.

515   Tan, J., Fu, J. S., Dentener, F., Sun, J., Emmons, L., Tilmes, S., Flemming, J., Takemura, T.,
516   Bian, H., Zhu, Q., Yang, C.-E., and Keating, T.: Source contributions to sulfur and nitrogen
517   deposition – an HTAP II multi-model study on hemispheric transport, Atmospheric Chemistry
518   and Physics, 18, 12223–12240, https://doi.org/10.5194/acp-18-12223-2018, 2018b.

519   Tørseth, K., Aas, W., Breivik, K., Fjæraa, A. M., Fiebig, M., Hjellbrekke, A. G., Lund Myhre,
520   C., Solberg, S., and Yttri, K. E.: Introduction to the European Monitoring and Evaluation
521   Programme (EMEP) and observed atmospheric composition change during 1972 - 2009,
522   Atmospheric Chemistry and Physics, 12, 5447–5481, https://doi.org/10.5194/acp-12-5447-2012,
523   2012.

524   Clean Air Status and Trends Network (CASTNET): https://www.epa.gov/castnet, last access: 18
525   November 2021.

526   Vet, R., Artz, R. S., Carou, S., Shaw, M., Ro, C.-U., Aas, W., Baker, A., Bowersox, V. C.,
527   Dentener, F., Galy-Lacaux, C., Hou, A., Pienaar, J. J., Gillett, R., Forti, M. C., Gromov, S., Hara,
528   H., Khodzher, T., Mahowald, N. M., Nickovic, S., Rao, P. S. P., and Reid, N. W.: A global
529   assessment of precipitation chemistry and deposition of sulfur, nitrogen, sea salt, base cations,
530   organic acids, acidity and pH, and phosphorus, Atmospheric Environment, 93, 3–100,
531   https://doi.org/10.1016/j.atmosenv.2013.10.060, 2014.

532   de Vries, W., Solberg, S., Dobbertin, M., Sterba, H., Laubhann, D., van Oijen, M., Evans, C.,
533   Gundersen, P., Kros, J., Wamelink, G. W. W., Reinds, G. J., and Sutton, M. A.: The impact of
534   nitrogen deposition on carbon sequestration by European forests and heathlands, Forest Ecology
535   and Management, 258, 1814–1823, https://doi.org/10.1016/j.foreco.2009.02.034, 2009.

536   Walker, J. T., Beachley, G., Amos, H. M., Baron, J. S., Bash, J., Baumgardner, R., Bell, M. D.,
537   Benedict, K. B., Chen, X., Clow, D. W., Cole, A., Coughlin, J. G., Cruz, K., Daly, R. W.,
538   Decina, S. M., Elliott, E. M., Fenn, M. E., Ganzeveld, L., Gebhart, K., Isil, S. S., Kerschner, B.
539   M., Larson, R. S., Lavery, T., Lear, G. G., Macy, T., Mast, M. A., Mishoe, K., Morris, K. H.,
540   Padgett, P. E., Pouyat, R. V., Puchalski, M., Pye, H. O. T., Rea, A. W., Rhodes, M. F., Rogers,
541   C. M., Saylor, R., Scheffe, R., Schichtel, B. A., Schwede, D. B., Sexstone, G. A., Sive, B. C.,
542   Sosa Echeverría, R., Templer, P. H., Thompson, T., Tong, D., Wetherbee, G. A., Whitlow, T. H.,
543   Wu, Z., Yu, Z., and Zhang, L.: Toward the improvement of total nitrogen deposition budgets in
544   the United States, Science of The Total Environment, 691, 1328–1352,
545   https://doi.org/10.1016/j.scitotenv.2019.07.058, 2019.

546   Wen, Z., Xu, W., Li, Q., Han, M., Tang, A., Zhang, Y., Luo, X., Shen, J., Wang, W., Li, K., Pan,
547   Y., Zhang, L., Li, W., Collett, J. L., Zhong, B., Wang, X., Goulding, K., Zhang, F., and Liu, X.:

548   Changes of nitrogen deposition in China from 1980 to 2018, Environment International, 144,
549   106022, https://doi.org/10.1016/j.envint.2020.106022, 2020.

550   Xu, W., Luo, X. S., Pan, Y. P., Zhang, L., Tang, A. H., Shen, J. L., Zhang, Y., Li, K. H., Wu, Q.
551   H., Yang, D. W., Zhang, Y. Y., Xue, J., Li, W. Q., Li, Q. Q., Tang, L., Lu, S. H., Liang, T.,
552   Tong, Y. A., Liu, P., Zhang, Q., Xiong, Z. Q., Shi, X. J., Wu, L. H., Shi, W. Q., Tian, K., Zhong,
553   X. H., Shi, K., Tang, Q. Y., Zhang, L. J., Huang, J. L., He, C. E., Kuang, F. H., Zhu, B., Liu, H.,
554   Jin, X., Xin, Y. J., Shi, X. K., Du, E. Z., Dore, A. J., Tang, S., Collett, J. L., Goulding, K., Sun,
555   Y. X., Ren, J., Zhang, F. S., and Liu, X. J.: Quantifying atmospheric nitrogen deposition through
556   a nationwide monitoring network across China, Atmos. Chem. Phys., 15, 12345–12360,
557   https://doi.org/10.5194/acp-15-12345-2015, 2015.

558   Xu, W., Zhang, L., and Liu, X.: A database of atmospheric nitrogen concentration and deposition
559   from the nationwide monitoring network in China, Sci Data, 6, 51,
560   https://doi.org/10.1038/s41597-019-0061-2, 2019.

561   Zhang, M., Leon, C. de, and Migliaccio, K.: Evaluation and comparison of interpolated gauge
562   rainfall data and gridded rainfall data in Florida, USA, Hydrological Sciences Journal, 63, 561–
563   582, https://doi.org/10.1080/02626667.2018.1444767, 2018.

564   Zhang, Y., Foley, K. M., Schwede, D. B., Bash, J. O., Pinto, J. P., and Dennis, R. L.: A
565   Measurement-Model Fusion Approach for Improved Wet Deposition Maps and Trends, Journal
566   of Geophysical Research: Atmospheres, 124, 4237–4251,
567   https://doi.org/10.1029/2018JD029051, 2019.

568   Zhao, Y., Zhang, L., Chen, Y., Liu, X., Xu, W., Pan, Y., and Duan, L.: Atmospheric nitrogen
569   deposition to China: A model analysis on nitrogen budget and critical load exceedance,
570   Atmospheric Environment, 153, 32–40, https://doi.org/10.1016/j.atmosenv.2017.01.018, 2017.

571   Zhu, J., Chen, Z., Wang, Q., Xu, L., He, N., Jia, Y., Zhang, Q., and Yu, G.: Potential transition in
572   the effects of atmospheric nitrogen deposition in China, Environmental Pollution, 258, 113739,
573   https://doi.org/10.1016/j.envpol.2019.113739, 2020.

574